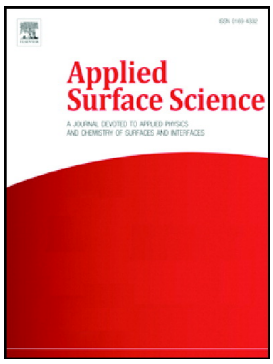

Fractal analysis of hillocks: A case of RF sputtered aluminum thin films

Fredrick M. Mwema, Esther T. Akinlabi, Oluseyi P. Oladijo

PII: S0169-4332(19)31660-5
DOI: https://doi.org/10.1016/j.apsusc.2019.05.340
Reference: APSUSC 42927

To appear in: *Applied Surface Science*

Received date: 28 January 2019
Revised date: 11 May 2019
Accepted date: 29 May 2019

Please cite this article as: F.M. Mwema, E.T. Akinlabi and O.P. Oladijo, Fractal analysis of hillocks: A case of RF sputtered aluminum thin films, Applied Surface Science, https://doi.org/10.1016/j.apsusc.2019.05.340

To be submitted to ANEM 2018-Australia: Applied Surface Science

Fractal Analysis of Hillocks: A case of RF Sputtered Aluminum Thin Films

Fredrick M. Mwema[1*], Esther T. Akinlabi[1] and Oluseyi P. Oladijo[1,2]

[1*]Department of Mechanical Engineering Science, University of Johannesburg, South Africa

[2]Department of Chemical, Materials and Metallurgical Engineering, Botswana International University of Science and Technology, Botswana, University

[*]fredrick.mwema@dkut.ac.ke, etakinlabi@gmail.com

Abstract

A monofractal and multifractal approach on quantification of hillocks on Al thin films deposited on glass substrates at a varying substrate temperature (T_s) have been reported in this work. The relationship between the fractal characteristics and mechanical properties of the hillocks are established. The lowest density and dimensions of hillocks were obtained at 95^{o}C while the highest at 65^{o}C. A power law relationship (with fractal dimension (D) as the power) is established between the perimeter and areas of the individual hillocks with a considerably large coefficient of regression ($R^2 \approx 0.9$) for all the temperatures. The fractal examinations of the segmented hillock structures revealed that these structures exhibit multifractal characteristics. The line profiles from optical profiling images of the hillock-dominant regions revealed non-uniform sinusoids which further confirm the fractal nature of these structures. The deformation mechanism of the hillocks under normal nanoindentation loading was described by evaluating the indentation impression against the nanoindentation curves.

Keywords: Aluminum thin films; hillocks; fractal dimension; image processing; multifractal; sputtering

Notations and Symbols

T_s: Substrate temperature

A: Area

ε: Dimension of the grids of the box-counting procedure

R^2: Coefficient of regression

N(ε): Number of grids

D: Fractal dimension

D(q): Generalized fractal dimension of the multifractal spectrum

C, k: Proportionality constants

L: Length scale

$P_{i,j}$: Probability of distribution of gray values in grid (i,j)

n_{ij}: Average height of the grids

α: Lipschitz-Holder/singularity strength exponent

f(α): Multifractal spectrum

q: Moment order

τ(q): Mass/correlation exponent

1. Introduction

Aluminum thin films are used as metallization networks in microelectronic systems and back contacts in thin solar cells [1], [2]. The main reason for their preference is the low cost, availability and easier fabrication of aluminum metal besides having low diffusivity, high contact conductivity and low sheet resistance[2], [3]. However, their applications (as pure Al) in electrical and solar systems are limited by microstructural defects such as pores, hillocks, and oxides. Hillocks are the most detrimental defects for electrical applications since they enhance electromigration in these films [4]–[6]. Hillocks manifest as large grains that outgrow all the other features of the surface and are attributed to various phenomena including thermal stress, oxidation, electromigration and external stress [4], [7]. Hillocks usually occur whenever there is a large mismatch between the thermal expansion of the Al films and nonmetallic substrates such as glass, silicon, and polymers [6]. Due to their significance in the functionality of thin films (including Al films), hillocks' evolution and analyses have been reported by various researchers. Zaborowski, Adamiec and Barcz [4] developed a procedural and reproducible technique for identification and statistical evaluation of hillocks on Al thin films using digital image processing. Fractal analyses of hillocks on palladium thin films and GaN surfaces have been reported [7], [8]. Through SEM imaging, the addition of Ni into Al thin films was shown to reduce hillock formation [9]. A similar method was used to study the effect of capping thicknesses on the suppression of hillocks in Al films [10]. Kikuchi pattern method of TEM micrographs was used to study the evolution of hillocks during annealing of Al-1%Si films [11]. From most of these studies, statistical analyses were employed to quantify the structural and morphological evolution of the micrographs of the hillocks [5]. Because of the significance of these structures in the performance of Al and other thin films, new and novel methods of quantification are of interest.

The objective of this article is to demonstrate the use of monofractal and multifractal analysis in studying the evolution hillocks in Al thin films deposited on glass substrates through sputtering at varying low substrate temperature (Ts). The hillocks analyzed in this work were attributed to oxidation and mismatch in thermal properties between the substrate and the metallization films. The structures of the hillocks were imaged by field emission scanning electron microscope (FESEM) and their fractal analyses were undertaken. The behavior of the hillocks under normal indentation loads was also evaluated and a relationship between fractal behavior and mechanical properties established. We observe that multifractal analyses and interrelationships between mechanical properties of hillocks and fractal characteristics are limited in literature, therefore making the current work novel and unique.

2. Experiments

The aluminum thin films were deposited on glass substrates by rf magnetron sputtering method at varying low substrate temperatures of 55^{o}C, 65^{o}C and 95^{o}C for a constant time of 2 hours and rf power was maintained at 350 W. The sputtering system and process used in this work has been described in details in our earlier publication [12], [13]. Prior to sputtering, the glass slides (substrates) were washed in distilled water and then acetone and dried on high-pressure and hot air. A high-purity Al target (99.99%) was mounted at a separation distance of 130 mm from the sample holders. The surface of the substrates was deionized by argon plasma by pre-sputtering for 10 minutes before deposition.

After the deposition, the samples were left to cool slowly inside the vacuum chamber for 3 hours. To observe and study the hillocks in these samples, the surfaces were imaged in a field emission scanning electron microscope (FESEM, ZEISS Gemini2). To recognize and analyze the hillocks, image processing method similar to that developed by Zaborowski *et al.* [4] was applied on the FESEM micrographs. The surface topographies (at microscale level) of the Al films containing hillocks were analyzed using bench-automated 3D optical profilometer (Contour Elite, Bruker, Massachusetts, USA). The topographies were analyzed in Vision64 Map® software. The roughness parameters were computed according to ISO 25178-2012 standards. The thicknesses of the films were also determined by the 3D optical profiler. The atomic force microscope (AFM) was used to analyze the nanoscale roughness properties of the films. The AFM measurements were conducted at a scan area of 5×5 μm^2 using Veeco 3100 AFM and the details of this facility are described elsewhere [12], [13]. The nanoindentation was undertaken on the surfaces using Ultra-Nanoindentation Tester

(UNHT³) (Anton Paar GmbH, Austria). Two sets of nanoindentation measurements were undertaken: (1) indentation was measured over the surface of the films for 15 points and their average values of moduli were reported for consistency and (2) indentation was carried out specifically on the hillock structures.

3. Fractal theory

In a mono-fractal analysis of surfaces and structures, fractal dimension (D) is the most significant parameter. Several techniques are available for determining fractal dimensions some of which include power spectral density, box counting, triangulation, autocorrelation and height-height correlation functions and among others. Fractal dimension measures the complex nature of structures and it is used as an analytical index to measure how the morphological features vary on scaling [14].

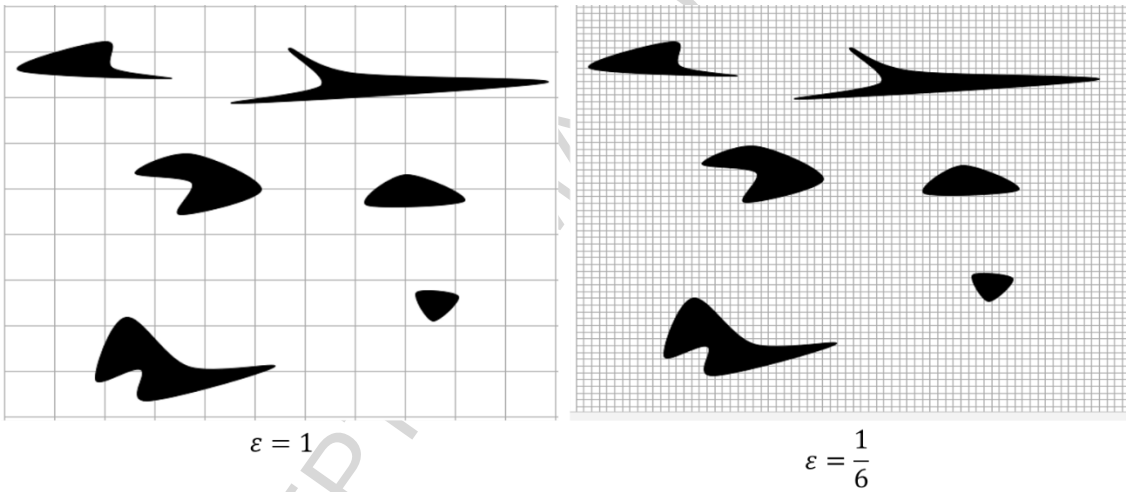

Figure 1. Schematic illustration of box-counting method where the left image shows grids of one unit while the right image shows grids of 1/6 unit. The smaller the size of the grids the more the number of grids and the more accurate the value of the fractal dimension. An optimal number of grids N(ε) should be determined to reduce the computation time.

Box-counting method is the most suitable for evaluation of the fractal dimension of isolated structures such as pores, corroded surfaces, hillocks and phases in microstructures [7], [15]. Box counting method, also known as cube counting, is illustrated in Fig. 1 above. As shown, the dark parts indicate the microstructural features under investigation. In box counting, each binary image is covered by a series of grids and for each of the grid, the number of square grids required to recover the area (hillocks) and the side length of the square gird is recorded [16]. Conventionally, the size of each grid is denoted as $\boldsymbol{\varepsilon}$ and the

number of grids as N(ε). The mathematical definition of fractal dimension D from the box counting technique is as follows.

$$D = \lim_{\varepsilon \to 0} \frac{\ln N(\varepsilon)}{\ln(\frac{1}{\varepsilon})} \quad (1)$$

For a fractal structure, the following relationship exists:

$$N(\boldsymbol{\varepsilon}) = C\boldsymbol{\varepsilon}^{-D} \quad (2)$$

Where C is constant of proportionality and D is the fractal dimension. Equation (1) can be rewritten in terms of the natural logarithm as follows. Equation (3) forms the linear regression for the solution to Equation (1) and a plot of $\ln[N(\boldsymbol{\varepsilon})]$ against $\ln(\boldsymbol{\varepsilon})$ and using least square fitting the slope of the plot gives the value of the fractal dimension D [15], [17].

$$\ln[N(\boldsymbol{\varepsilon})] = \ln(C) - D\ln(\boldsymbol{\varepsilon}) \quad (3)$$

In most structures, the scaling behavior may change from one point to another and as such mono-fractal analysis is no longer valid and therefore multifractal approach is recommended. In this approach, the most important is the multifractal spectrum and we adopted the approach used by Xu *et al.*[15] and Liu *et al.*[18] described as follows. We denote that for the box counting illustrated in Fig. 1 $\varepsilon = l/L \leq 1$ is valid. Where l and L represents the length scale and upper bound on the scale respectively [18].

$$P_{ij}(\varepsilon) = \frac{n_{ij}}{\sum n_{ij}} \quad (4)$$

Where $P_{ij}(\varepsilon)$ represents the average probability of distribution of the gray values in the grid(i,j) and n_{ij} is the average height of the grid (or gray values) of size ε. For a multifractal description of the box(i,j) within the scale ε, P_{ij} can be related to ε as follows.

$$P_{ij}(\varepsilon) \propto \varepsilon^{\alpha} \quad (5)$$

Where exponent α is the singularity of the subset of probabilities and depends on the box(i,j). It is also known as Lipschitz-Holder exponent or singularity strength function. When all the boxes have the same α the surface is said to be mono-fractal, otherwise, the microstructure is multifractal. The number of boxes with the same probability of gray value distribution have the following relationship.

$$N(\boldsymbol{\varepsilon}) \propto \boldsymbol{\varepsilon}^{-f(\alpha)} \quad (6)$$

Where f(α) is the singularity spectrum and it is a continuous function of α. The singularity spectrum can be determined by a partition function (Z(q,**ε**) as follows.

$$Z(q,\varepsilon) = \sum P_{ij}^{q}(q) = \varepsilon^{\tau(q)} \quad (7)$$

From Equation (7), q is a real parameter (-∞<q<∞) known as the moment order while τ(q) is the mass or correlation exponent which can be determined from the slope of the curve of ln[Z(q,ε)] versus ln(ε). If the parameter q can be viewed as a microscope (since it differentiates between two similar maps) and the size of boxes ε as the filter, then Z(q, ε) would provide information at different scales and moment order. In that case, the spectrum function f(α) can be computed using the Legendre transform as shown in Equation (8).

$$f(\alpha(q)) = \alpha(q)q - \tau(q) = q\frac{d\tau(q)}{dq} - \tau(q) \quad (8)$$

A plot of f(α) against α yields a continuous function known as the multifractal spectrum from which various multifractal measures can be extracted to explain the evolution of physical process such as the formation of hillocks. The generalized dimension D(q) which describes the mass variation with the size of grids (ε) is computed from the mass exponent function as shown in Equation (9).

$$D(q) = \frac{\tau(q)}{q-1} \quad (9)$$

When the structure is mono-fractal, a plot of D(q) against q exhibits a non-increasing behavior or simply horizontal, however, when it is multifractal, the plot exhibit decreasing and sigmoidal behavior [15]. In this work, these equations were implemented in the open source plugin *FracLac* tool in *ImageJ* software.

4. Results and Discussion

The thickness of the films measured by the 3D optical surface profilometry was 500-600 nm; the thickness of the films is not expected to change since the sputtering was undertaken at the constant time of 2 hours and similar results have been reported for Al-Mg-B films [19]. Fig. 2 shows the FESEM micrographs of the Al thin films sputtered on glass substrates at different substrate temperatures. The hillocks structures are indicated by the white arrows in the micrograph and they appeared as nodules or condensed lumps of structures. At 55^{o}C (Fig. 2a), few, small and circular hillocks were observed while at 65^{o}C, many larger and interconnected hillocks were present as seen in Fig. 2b. At 95^{o}C (Fig. 2c), very few and tiny hillocks were observed in the microstructure. The difference in morphology

of the hillocks can be attributed to T_s and surface oxidation which readily occurs on pure Al films. The FESEM observations are comparable to those of the AFM microscopy shown in Appendix 1. To undertake a quantitative analysis of the hillock structures, images in Fig. 3 obtained through image segmentation and procedure described by Zaborowski *et al.* [4] were used. Fig. 3 shows the images in Fig. 2 after image processing. The detailed measurements of the hillocks in the microstructures at different substrate temperature are shown in Table 1. The size descriptors such as percentage area fraction (%A), perimeter (P) and ferret number showed the largest sizes of hillocks were formed at 65^{o}C while the smallest sizes were observed at 95^{o}C. The results are attributed to nonuniform development of grains at the initial increase in substrate temperature as reported in literature [20]. The shape descriptor, sphericity, in this case, was highest for films containing the smallest size of the hillocks and lowest in the films containing the largest sizes of hillocks (at 65^{o}C).

Table 1

Size measurements and physical law relating areas and perimeters of hillocks in Al thin films. The raw data leading to the information presented in this table is attached as Appendices 2, 3, 5

Specimen (T_s)	Area fraction, A (%)	Perimeter, P (nm)	Correlation power law; $P=kA^{(D-1)}$, where D is the fractal dimension and k is the constant of proportionality	R^2, Correlation coefficient of fit between perimeter and area	Ferret size (nm)	Sphericity
55^{o}C	0.352	70.07	$P=2.233A^{0.58}$	0.9662	29.30	0.965
65^{o}C	0.918	96.76	$P=2.300A^{0.59}$	0.8523	40.05	0.698
95^{o}C	0.326	63.25	$P=1.754A^{0.62}$	0.9238	27.35	0.978

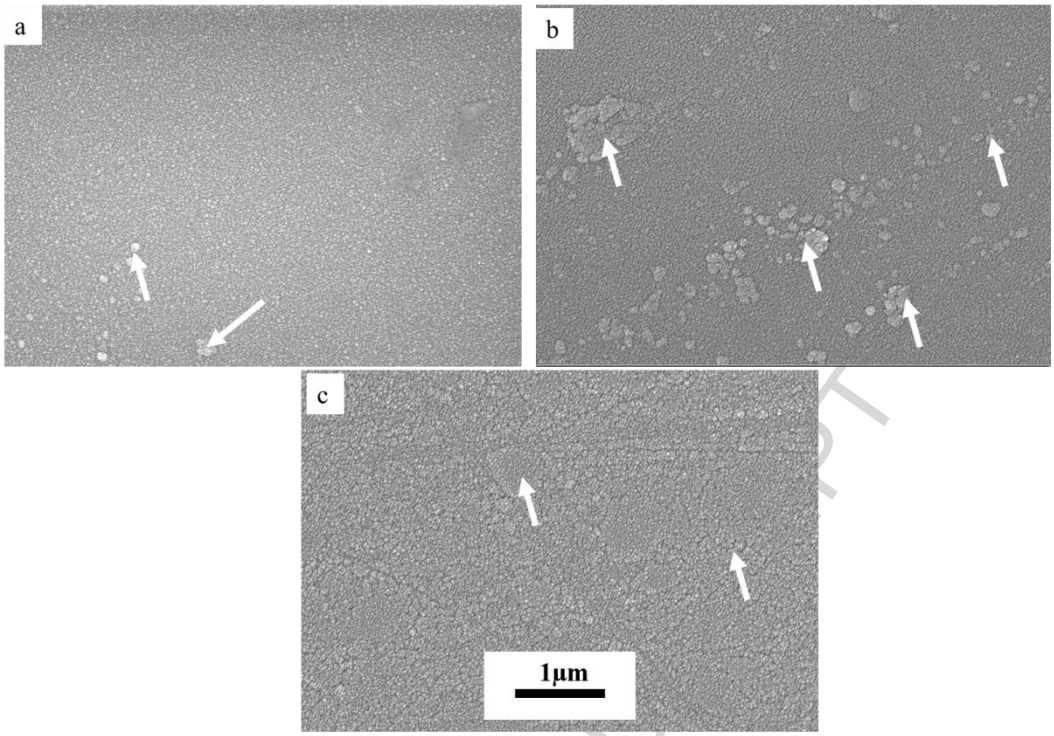

Figure 2. Representative FESEM micrographs of Al thin films deposited on glass substrates at different substrate temperatures (a) 55°C (b) 65°C and (c) 95°C. The white arrows indicate hillock structures present in these films.

The individual surface areas and perimeters of the hillocks for each T_s were measured as indicated in Table 1. As described in reference [7], when the hillocks are characterized by surface area (A), the area is related to the equivalent circle radius while the perimeter (P) of the hillocks is related to the fractal dimension (D) of the thin film. A plot of P against A (shown in Appendices 1, 2 and 3) where each point on the plot represent a hillock on the surface of films at each substrate temperature, shows a mathematical relation described by a power law according to Equation (10). These plots (P versus A) indicate the dimensionality and size distributions of the hillock structures within the microstructure of the Al thin films at various T_s.

$$P = kA^{D-1} \tag{10}$$

Where k and D represent the constant of proportionality between P and A and fractal dimension of the hillock's distribution respectively. The power law correlations for the three specimens are shown in Table 1 and the correlations obey the relationship in Equation (10) at sufficiently high values of R^2. The lowest value of R^2 obtained at 65°C can be attributed to the microstructural observation of large, irregular and interconnected hillock structures. From the relationship, the fractal dimensions for the hillocks were determined as 1.58, 1.59 and

1.62 for films deposited at 55°C, 65°C and 95°C respectively. A similar relationship was reported for hillocks formed due to oxidation of palladium thin films [7].

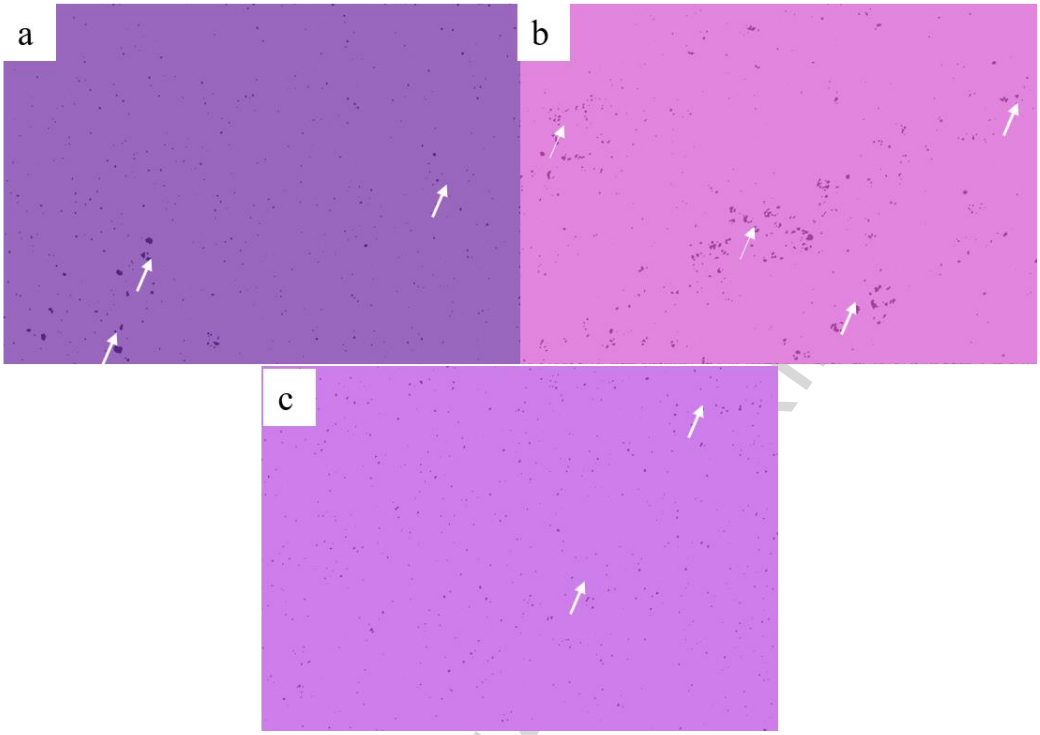

Figure 3. Illustrating hillock recognition through binary image processing for the images of films deposited at substrate temperatures of (a) 55°C (b) 65°C and (c) 95°C (The same images are shown in Fig. 2 before image processing). The images have been segmented for recognition and further analysis of the hillock structures some of which are indicated by white arrows.

The computation of fractal dimension (based on box counting method) and the multifractal spectrum was performed, and the obtained values of related parameters summarized in Table 2. The values of D obtained by the box-counting method (Equations (1)-(3)) are comparable to those obtained by Equation (10) although the latter values are higher. The differences between the values is attributed to the discrepancies in the accuracies of the two computations methods in which box-counting methods is depended on the number of boxes whereas the P-A method depends on the image segmentation process. Different computation methods usually give different values of D and therefore the need to utilize several techniques in this study [21], [22]. Because of these differences, we performed a convergence study on the box counting method to understand the range of the D values of these hillocks. Fig. 4 shows the results of that convergence study and indicates that 500 was the optimum number of boxes to compute the value of D for all the films. At N(ε)=500, the coefficient of correlation of linear regression for the three specimens was ~0.99, which

implies that the distribution of hillocks in sputtered Al films on glass substrate within T_s range of 55-95^{o}C exhibits a statistical fractal feature.

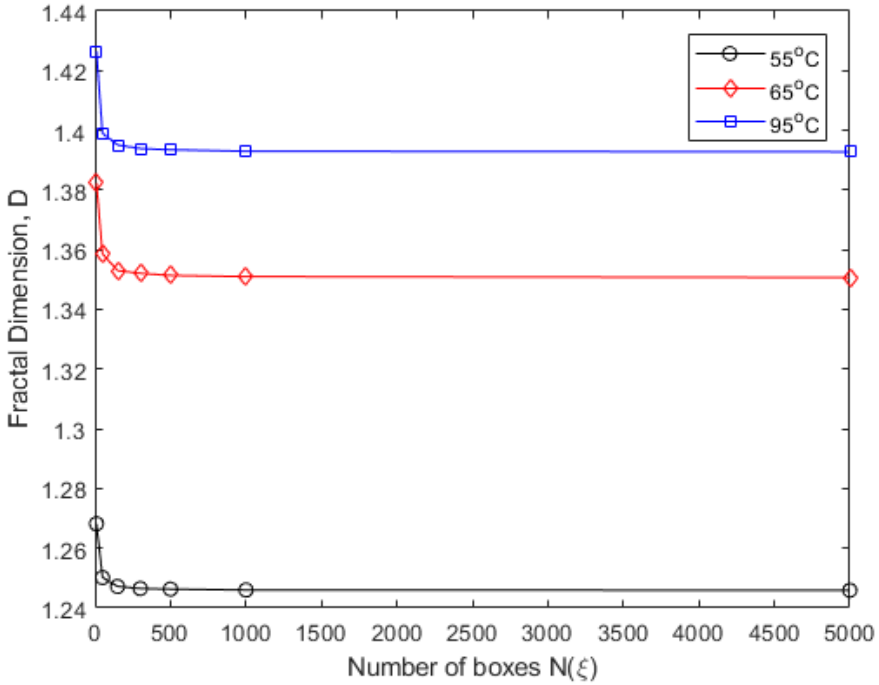

Figure 4. Convergence analysis for determining the optimal number of grids, N(ε), during the computation of fractal dimensions by box counting method. As observed, the solutions converged after 500 grids for all the samples. These results justify the choice of 500 grids in all the fractal analyses.

Multifractal analysis is used to eliminate the effects of changes in data sets from one point to another. The mass exponent (also known as multifractal scaling exponent, τ(q)) was computed using Equation (7) for -10<q<10 and the results plotted as a function of q as shown in Fig. 5 for all the specimens. For all the plots, τ(q) exhibit nonlinear increase with q, which confirms that the hillocks analyzed in these films are multifractal in nature [23]. As observed, at q=-10, the hillocks on films deposited at T_s of 65^{o}C showed the minimum value of τ(q)=-18 while the maximum value of τ(q)=-22 was obtained for 55^{o}C. The point of inflection for all the films was observed q=1 where all the values of τ(q). At q=10, the highest value of τ(q) was obtained at 95^{o}C and lowest at 55^{o}C. Generally, the highest deviation of linearity was observed at films deposited at 65^{o}C which can be attributed to large, irregular and interconnected (rough) hillocks formed on these films as earlier observed in the FESEM micrographs.

The most significant parameters for describing multifractality of structures are multifractal spectrum f(α) and singularity strength exponent α which were computed

according to Equation (8). Fig. 6 shows f(α) versus α for the films deposited at various T_s. As seen, the curves exhibit similar shapes, different widths, and peaks. As the %A of hillocks increase (at 95^{o}C), the peaks of the multifractal spectrum shift to the right. Furthermore, the maximum peak of the spectra was observed on the films containing the largest sizes of hillocks (95^{o}C). All the spectra are humped with hooks to the right, which indicates the existence of multifractal behavior of the hillock structures in the Al films. The parameters of the multifractal spectrum obtained from Fig. 6 are summarized in Table 2. The α_{min} and α_{max} values correspond to the least and most singular strengths respectively while the corresponding spectral values (or fractal dimensions) for these regions are $f(\alpha_{min})$ and $f(\alpha_{max})$. The Δα measures the width of the multifractal spectrum and in this case, the lowest value was obtained on the films containing small sizes (and density) of hillocks, i.e. the films deposited at 95^{o}C. Strictly speaking, the larger the value of Δα the rougher and more irregular the surface under investigation [24]. The highest of Δf(α) was obtained at 95^{o}C while the lowest at 65^{o}C, which means that at 65^{o}C, the surface of the Al films consists of rough and well-developed hillock structures and smooth and complex structure at 95^{o}C. Additionally, all the values of Δf(α) were greater than 0, implying that distribution of hillocks are depended on the maximum subset of probability. These results agree with the fractal and microstructural observations. In formulating multifractal problems, α_{min} relates to the maximum indicator of probability (p_{max}) as $p_{max} \propto \varepsilon^{\alpha_{min}}$ where the scale $\varepsilon \to 0$ and vice versa for p_{min} [23]. As such, Δα is used in explaining the range of measures of probability as $\frac{p_{max}}{p_{min}} = \varepsilon^{-\Delta\alpha}$. In this case, the reduction in Δα resulting in decrease in width of probability distribution indicating that the hillocks development with low T_s of Al films sputtered on glass substrates exhibit a multifractal behavior.

The plots generalized dimension D(q) against moment order q are represented in Fig. 7. The computation of D(q) was based on Equation (9). For all the T_s, the D(q) function decreased with q, which further confirms the multifractality of the hillock in these films. The results are consistent with those presented for corrosion structures in steel [15]. However, the plots (D(q) versus q) are significantly different from those reported by Muller *et al.*[25] for porosity description of sedimentary rocks. The most important parameters of this function namely D(0), D(1), D(2) and W=D(0)-D(1) are summarized in Table 2. D(0) denotes the capacity dimension, D(1) is the fractal dimension of the hillocks and D(2) is the correlation fractal dimension. For all the films, D(0)>D(1)>D(2). The values of D(1) obtained in are comparable to the fractal values obtained through the monofractal analysis. The value of W is

used to illustrate the multifractal spectra and large values of W indicate the presence of a large and heterogeneous distribution of the hillock structures in the microstructure. A similar argument was presented for multifractality analysis of porous media [26]. These results agree with the multifractal spectra and the FESEM observations discussed earlier.

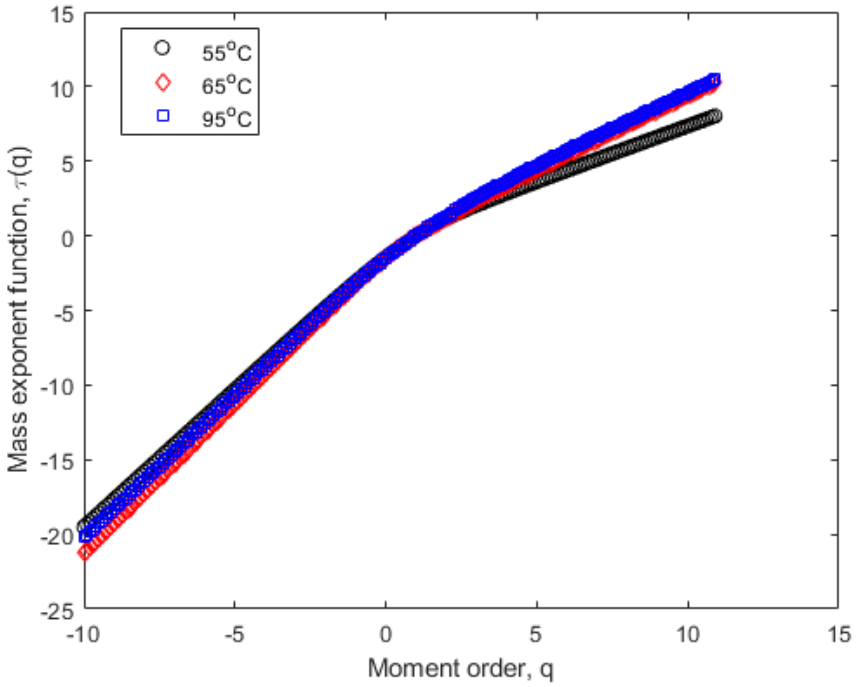

Figure 5. Plots of mass exponent τ(q) versus moment order (q) for the hillock structures on the three films.

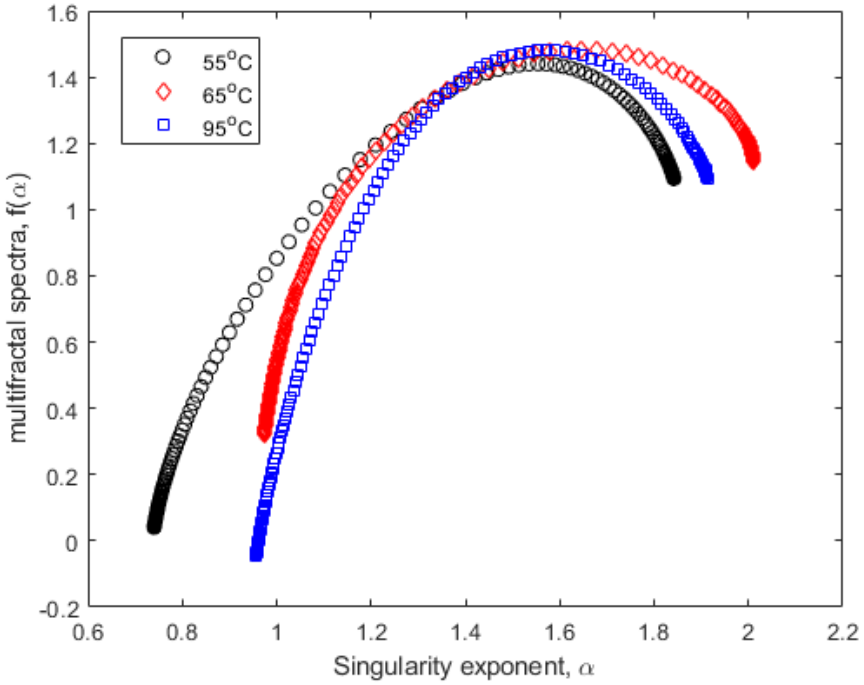

Figure 6. The multifractal spectra of the hillock structures in Al thin films deposited at various substrate temperatures viz. 55°C, 65°C and 95°C.

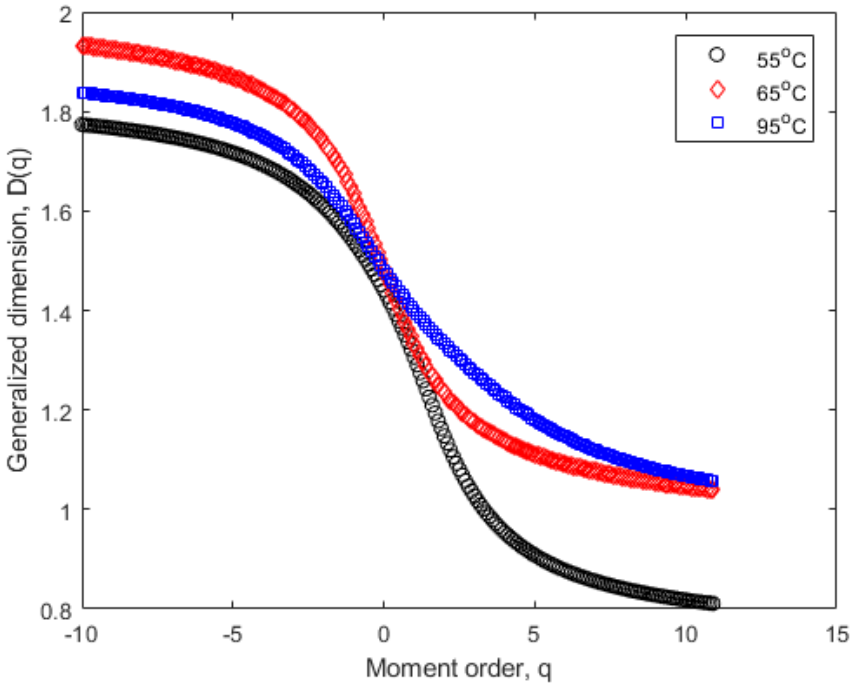

Figure 7. Generalized dimensions spectra D(q) for various samples plotted against moment order (q) at ranges of −10 to 10 and evaluated at increments of 0.2

Table 2

Fractal parameters describing the distribution of hillocks in thin Al films sputtered on glass substrates

Specimens	D	α_{min}	α_{max}	$\Delta\alpha$	$f(\alpha_{max})$	$f(\alpha_{min})$	$\Delta f(\alpha)$	D(0)	D(1)	D(2)	W
55°C	1.2463±0.0083	0.7403	1.842	1.1017	1.469	0.04046	1.42854	1.44	1.306	1.148	0.134
65°C	1.3514±0.0109	0.9737	2.011	1.0373	1.4841	0.3199	1.1642	1.484	1.335	1.234	0.149
95°C	1.3935±0.0112	0.9564	1.913	0.9566	1.4822	-0.04677	1.52897	1.482	1.4	1.33	0.082

Fig. 8 shows the topography of the hillocks imaged by a 3D non-contact optical surface profilometer. Initially, the global surface roughness of the films was computed by scanning an area of 3000 μm^2 (Figures not shown). The global average roughness (Ra) values were obtained as 183, 244 and 173 nm for Al films deposited at 55°C, 65°C, and 95°C respectively whereas the root means square roughness (Rq) were computed as 194, 200 and 188 nm respectively. These results indicate that the roughness of Al thin films increased with the size and density of the hillocks. The local imaging (Fig.8) shows that at 55°C, the hillock-dominated regions exhibited sinusoidal topography as seen on the line profile Fig. 8(a). The interconnected hillock structures as observed in FESEM micrographs at 65°C are responsible for the topography observed in Fig. 8(b) whereas the presence of small and few hillock structures at 95°C led to considerably uniform topography as seen in Fig. 8(c). The optical surface profiler (OSP) captures the arrangement of the surface structures which can be attributed to the microstructural arrangement (at high resolutions) as observed via advanced techniques such as FESEM. As such, the surface roughness obtained by OSP can be attributed to the nature of the microstructural features obtained through FESEM. Furthermore, in fractal surfaces, although the scale of measurements can show different resolutions and details, the arrangement of the surface structures and hence the holistic nature of surfaces remains the same.

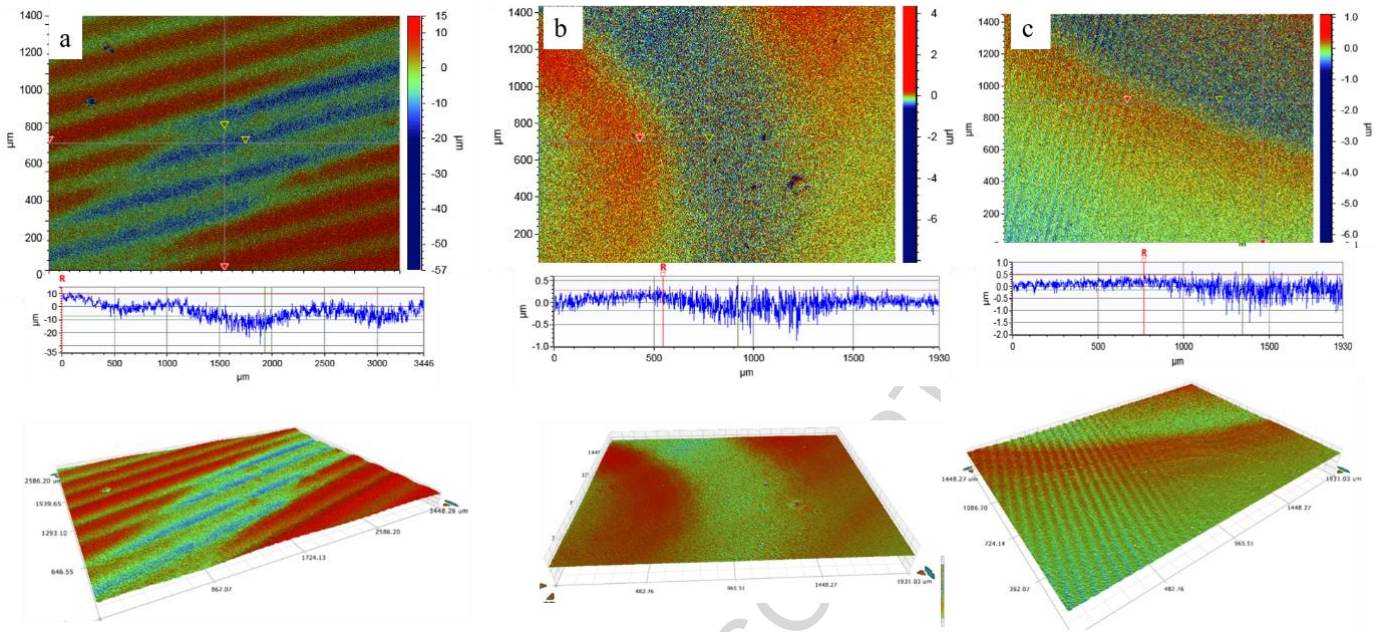

Figure 8. Non-contact optical surface profiling of various hillock structures on Al thin films sputtered on glass substrates at different substrate temperatures (a) 55^{o}C (b) 65^{o}C and (c) 95^{o}C. 2D images and their corresponding 3D images are shown. The line profiles are extracted along the regions of high concentrations of hillocks to give visual and quantitative morphological measurements of the hillocks.

The reduced moduli for the Al films in this study (an average of 15 points) were obtained as 135.1±0.0013, 110.6±0.024 and 145.5±0.0010 GPa for the 55^{o}C, 65^{o}C, and 95^{o}C films respectively. These results indicate that films with high concentration and large sizes of hillocks exhibited the lowest and heterogenous mechanical properties. We further undertook indentation specifically on the hillock structures and the results are illustrated in Fig. 9 and 10. As observed in Fig. 9, all curves exhibited various break-up regions at loading beyond 0.03 mN. The highest elastic modulus (162.61 GPa) was obtained at 65^{o}C whereas the lowest (120.85 GPa) was determined at 55^{o}C. The hillock structures were hardest (549.74 MPa) at 95^{o}C while they were softest at 65^{o}C with the lowest hardness of 335.7 MPa. The visual observation of the Berkovich (diamond) indenter impression onto the hillock structures are also shown alongside the corresponding curves. For all the cases, unfamiliar circular impressions were observed indicating that the hillocks were undergoing severe plastic deformation and flow during the nanoindentation loading. The mechanism of their deformation can be thought of as a ‘hard-dough pile-up’ under slow-load pressing.

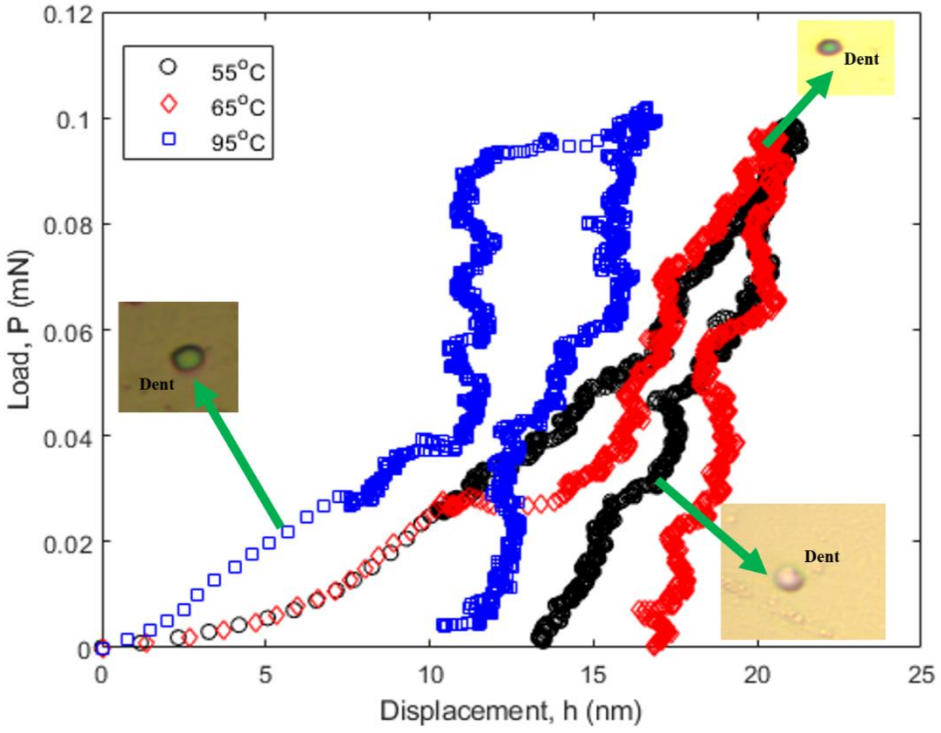

Figure 9. Nanoindentation curves (load, P versus displacement h) of the hillock structures on the different films.

5. Conclusions

The monofractal and multifractal analyses of hillocks in Al thin films deposited on glass substrates has been presented in this article. Through these approaches, the following conclusions can be drawn:

- The hillock formation is influenced by the low substrate temperature variation during magnetron sputtering. The smallest size of hillocks (area and perimeter) were observed at 95^{o}C with the largest determined at a substrate temperature of 65^{o}C.
- The line profiles extracted from the optical surface profilometry of the hillock-dominant regions of the micrographs might be associated with long wavelength surface variability (waviness) and fractal analyses into the FESEM micrographs revealed fractal nature of the surfaces. The multifractal spectrum, mass exponent and generalized fractal dimensions indicated that the surface hillocks are multifractal.
- From both monofractal and multifractal approaches, fractal dimensions (D) were determined. In all the cases, the values of D were seen to increase with the substrate temperature indicating that the complexity, growth and interconnection of the surface structures over hillocks from 55^{o}C to 95^{o}C. The values of the width of the multifractal spectra were obtained as 1.10, 1.03 and 0.96 indicating lateral growth of surface

roughness due to the preferential development of surface structures over the hillocks at higher temperature.

Acknowledgments

We acknowledge the university research committee (URC) of the University of Johannesburg for supporting the research student working on this subject. Indian Institute of Technology, IIT, is also acknowledged for granting access into their central research facility for characterization of the samples.

References

[1] M. Z. Pakhuruddin, K. Ibrahim, and A. A. Aziz, "Properties of Aluminium Thin Films on Polyethylene Terephthalate Substrates as Back Contacts in Thin Film Silicon Solar Cells," *Int. J. Polym. Mater.*, vol. 61, no. 9, pp. 669–678, 2012.

[2] F. M. D'Heurle, "Aluminum films deposited by rf sputtering," *Metall. Mater. Trans. B*, vol. 1, no. 3, pp. 725–732, 1970.

[3] S. . Kim, H. . Choi, and S. . Choi, "A study on the crystallographic orientation with residual stress and electrical property of Al films deposited by sputtering," *Thin Solid Films*, vol. 322, no. 1–2, pp. 298–302, 1998.

[4] M. Zaborowski, M. Adamiec, and A. Barcz, "Hillock recognition by digital image processing," *Appl. Surf. Sci.*, vol. 91, no. 1–4, pp. 246–250, 1995.

[5] S. J. Hwang, J. H. Lee, C. O. Jeong, and Y. C. Joo, "Effect of film thickness and annealing temperature on hillock distributions in pure Al films," *Scr. Mater.*, vol. 56, no. 1, pp. 17–20, 2007.

[6] F. M. Mwema, O. P. Oladijo, S. A. Akinlabi, and E. T. Akinlabi, "Properties of physically deposited thin aluminium film coatings: A review," *Journal of Alloys and Compounds*, vol. 747. pp. 306–323, 2018.

[7] S. Nazarpour and M. Chaker, "Fractal analysis of Palladium hillocks generated due to oxide formation," *Surf. Coatings Technol.*, vol. 206, no. 11–12, pp. 2991–2997, 2012.

[8] G. R. Mutta and S. Carapezzi, "2D scaling behavior of nanotextured GaN surfaces: A case study of hillocked and terraced surfaces," *Appl. Surf. Sci.*, vol. 447, pp. 845–851, 2018.

[9] K. W. Lee *et al.*, "Effects of a Ni alloying element on AlNi metallization," *Semicond. Sci. Technol.*, vol. 27, no. 1, 2012.

[10] K.-H. Jang, "Effect of Capping Layer on Hillock Formation in Thin Al Films," *Met. Mater. Int.*, vol. 14, no. 2, pp. 147–150, Apr. 2008.

[11] R. A. Schwarzer and D. Gerth, "The effect of grain orientation on the relaxation of thermomechanical stress and hillock growth in AI-1%Si conductor layers on silicon substrates," *J. Electron. Mater.*, vol. 22, no. 6, pp. 607–610, 1993.

[12] F. M. Mwema, O. P. Oladijo, and E. T. Akinlabi, "Effect of Substrate Temperature on Aluminium Thin Films Prepared byRF-Magnetron Sputtering," *Mater. Today Proc.*,

vol. 5, no. 9, pp. 20464–20473, 2018.

[13] F. M. Mwema, O. P. Oladijo, T. S. Sathiaraj, and E. T. Akinlabi, "Atomic force microscopy analysis of surface topography of pure thin aluminium films," *Mater. Res. Express*, vol. 5, no. 4, pp. 1–15, Apr. 2018.

[14] A. Annadhason, "Methods of Fractal Dimension Computation," *IRACST - International J. Comput. Sci. Inf. Technol. Secur.*, vol. 2, no. 1, pp. 2249–9555, 2012.

[15] Y. Xu, C. Qian, L. Pan, B. Wang, and C. Lou, "Comparing monofractal and multifractal analysis of corrosion damage evolution in reinforcing bars," *PLoS One*, vol. 7, no. 1, pp. 1–8, 2012.

[16] L. Wang, Z. Wang, W. Xie, and X. Song, "Fractal study on collective evolution of short fatigue cracks under complex stress conditions," *Int. J. Fatigue*, vol. 45, pp. 1–7, 2012.

[17] Y. D. Xu and C. X. Qian, "Fractal Characterization of Corroded Surface Profile in Reinforcing Steel Bars," *Adv. Mater. Res.*, vol. 163–167, pp. 3118–3121, 2010.

[18] C. Liu, X. L. Jiang, T. Liu, L. Zhao, W. X. Zhou, and W. K. Yuan, "Multifractal analysis of the fracture surfaces of foamed polypropylene/polyethylene blends," *Appl. Surf. Sci.*, vol. 255, no. 7, pp. 4239–4245, 2009.

[19] Z. Wu *et al.*, "Al-Mg-B thin films prepared by magnetron sputtering," *Vacuum*, vol. 85, no. 4, pp. 541–545, 2010.

[20] T. Kobayashi, H. Kitahara, and N. Hosokawa, "Substrate temperature dependence of hillock, grain, and crystal orientation in sputtered Al–alloy films," *J. Vac. Sci. Technol. A Vacuum, Surfaces, Film.*, vol. 5, no. 4, pp. 2088–2091, 1987.

[21] Ş. Tălu *et al.*, "Gold nanoparticles embedded in carbon film: Micromorphology analysis," *J. Ind. Eng. Chem.*, vol. 35, pp. 158–166, 2016.

[22] Ş. Ţălu, M. Bramowicz, S. Kulesza, and S. Solaymani, "Topographic characterization of thin film field-effect transistors of 2,6-diphenyl anthracene (DPA) by fractal and AFM analysis," *Mater. Sci. Semicond. Process.*, vol. 79, no. February, pp. 144–152, 2018.

[23] R. P. Yadav, S. Dwivedi, A. K. Mittal, M. Kumar, and A. C. Pandey, "Fractal and multifractal analysis of LiF thin film surface," *Appl. Surf. Sci.*, vol. 261, pp. 547–553, 2012.

[24] F. Hosseinpanahi, D. Raoufi, K. Ranjbarghanei, B. Karimi, R. Babaei, and E. Hasani, "Fractal features of CdTe thin films grown by RF magnetron sputtering," *Appl. Surf. Sci.*, vol. 357, pp. 1843–1848, 2015.

[25] J. Muller, O. K. Huseby, and A. Saucier, "Influence of multifractal scaling of pore geometry on permeabilities of sedimentary rocks," *Chaos, Solitons and Fractals*, vol. 5, no. 8, pp. 1485–1492, 1995.

[26] F. J. Jiménez-Hornero, E. Gutiérrez de Ravé, J. V. Giráldez, and A. M. Laguna, "The influence of the geometry of idealised porous media on the simulated flow velocity: A multifractal description," *Geoderma*, vol. 150, no. 1–2, pp. 196–201, 2009.

Appendix

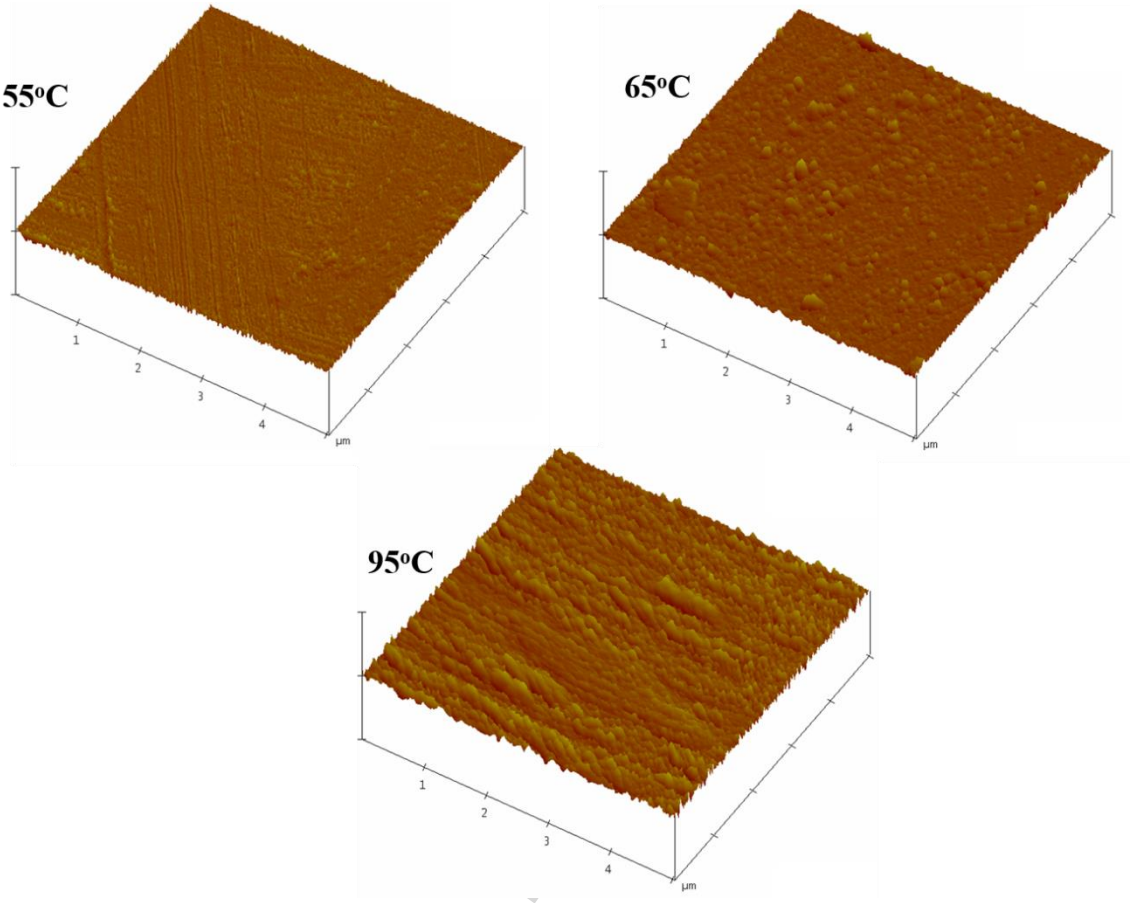

Appendix 1: 3D AFM micrographs revealing the hillocks. At 65°C, well-defined and round hillock structures are observed.

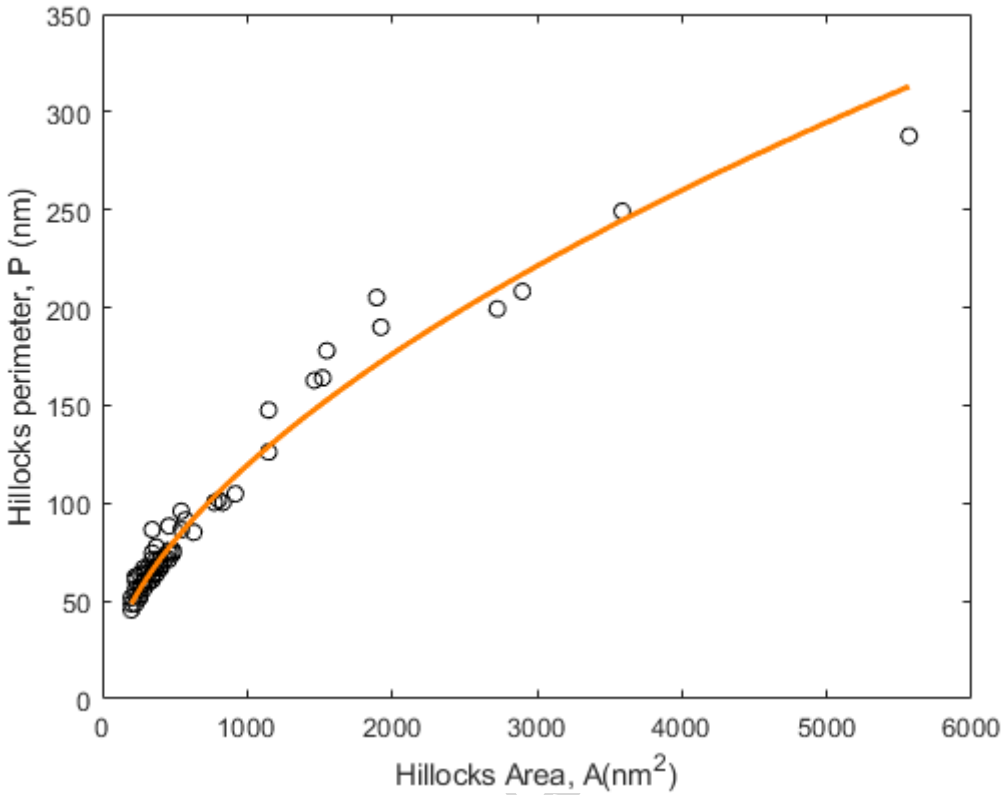

Appendix 2: Hillocks perimeter versus areas fitted with power law for thin films deposited at T_s=55^{o}C,

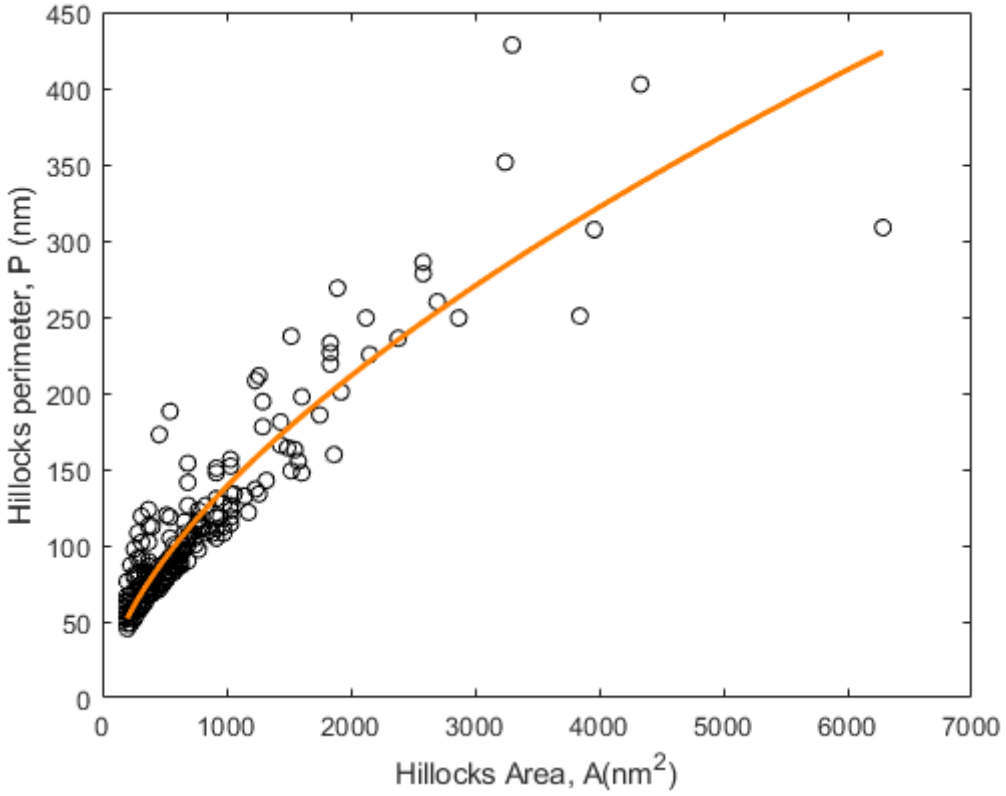

Appendix 3: Hillocks perimeter versus areas fitted with a power law of thin films deposited at T_s=65^{o}C

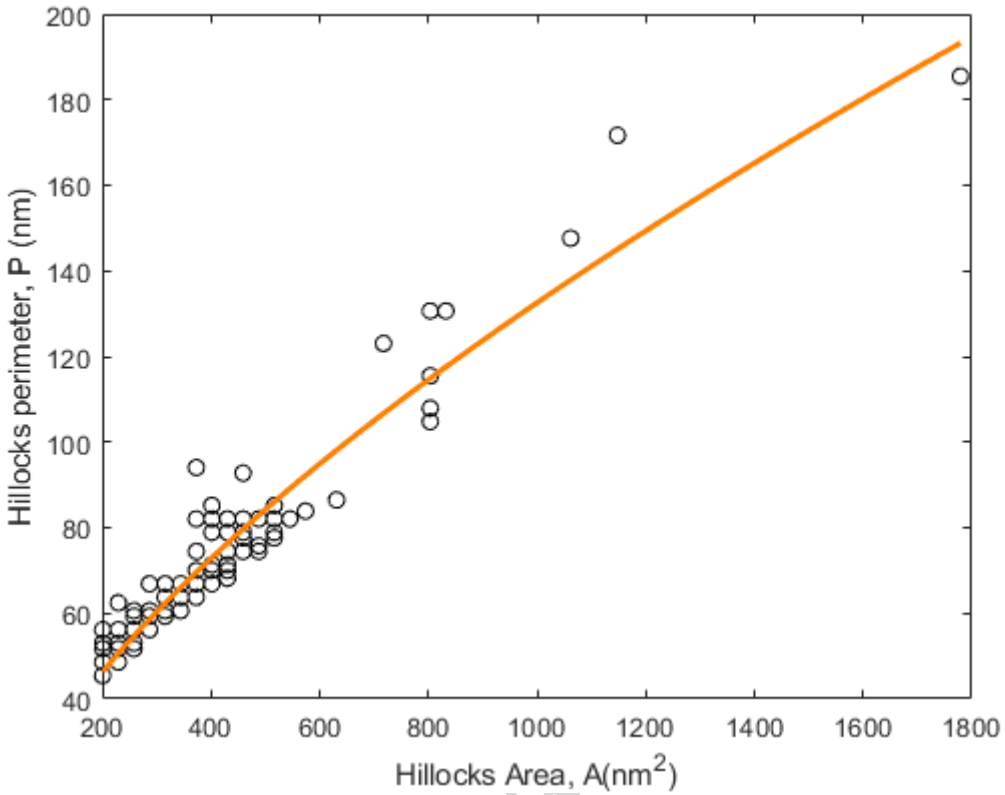

Appendix 4: Hillocks perimeter versus areas fitted with a power law of thin films deposited at T_s=95^{o}C

Highlights

- Aluminum thin films were deposited on glass substrates via RF magnetron sputtering at substrate temperature range of 55-95^{o}C
- Fractal techniques were used to analyze the microstructural evolution of the hillock structures obtained through FESEM
- The fractal results were related to the nanoindentation, AFM and profiling results and conclusions drawn

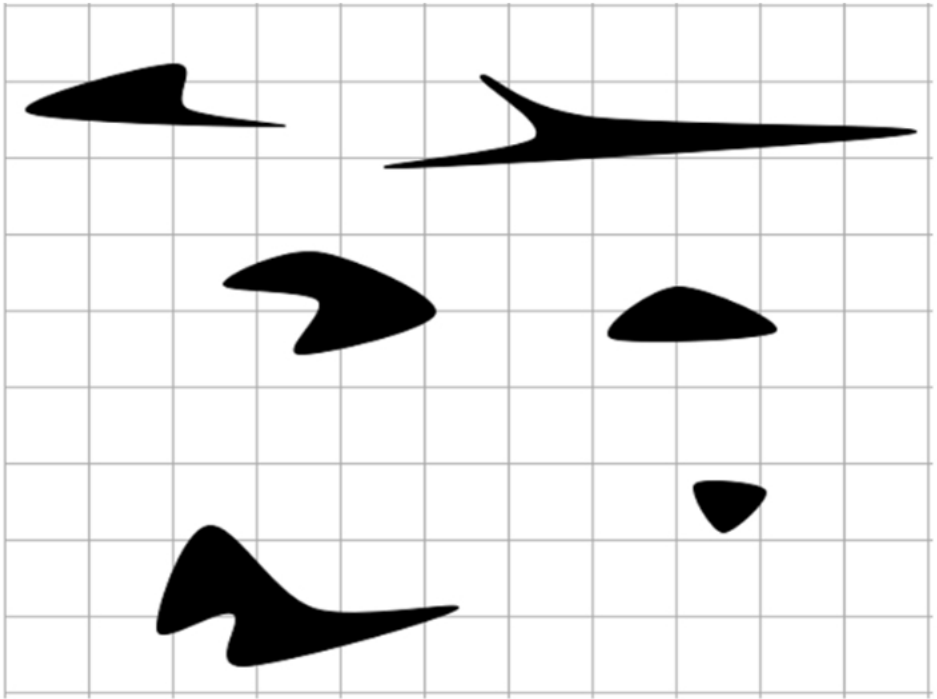

$\varepsilon = 1$

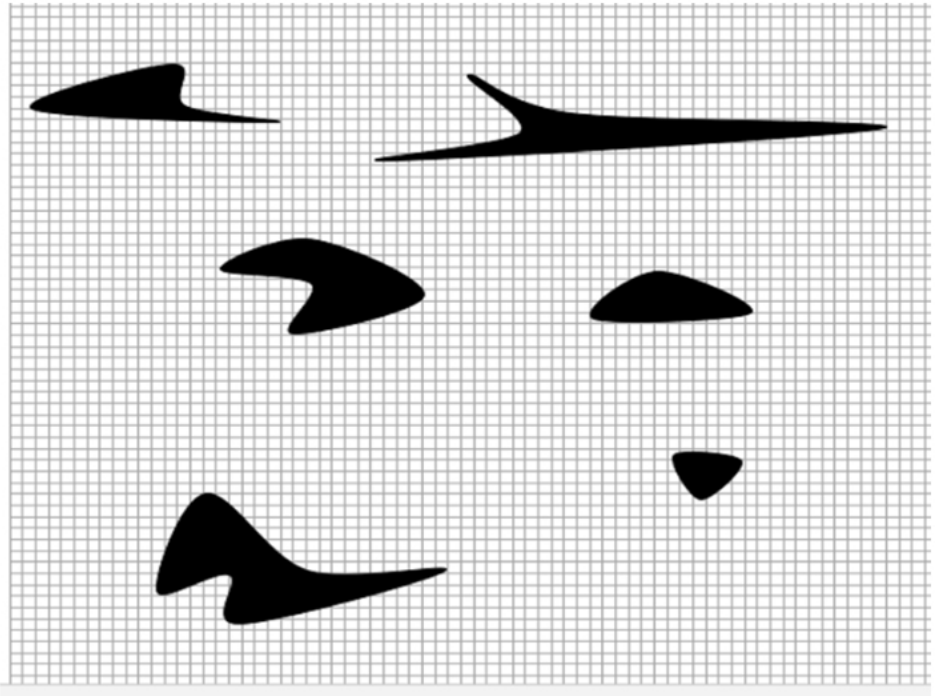

$\varepsilon = \frac{1}{6}$

Figure 1

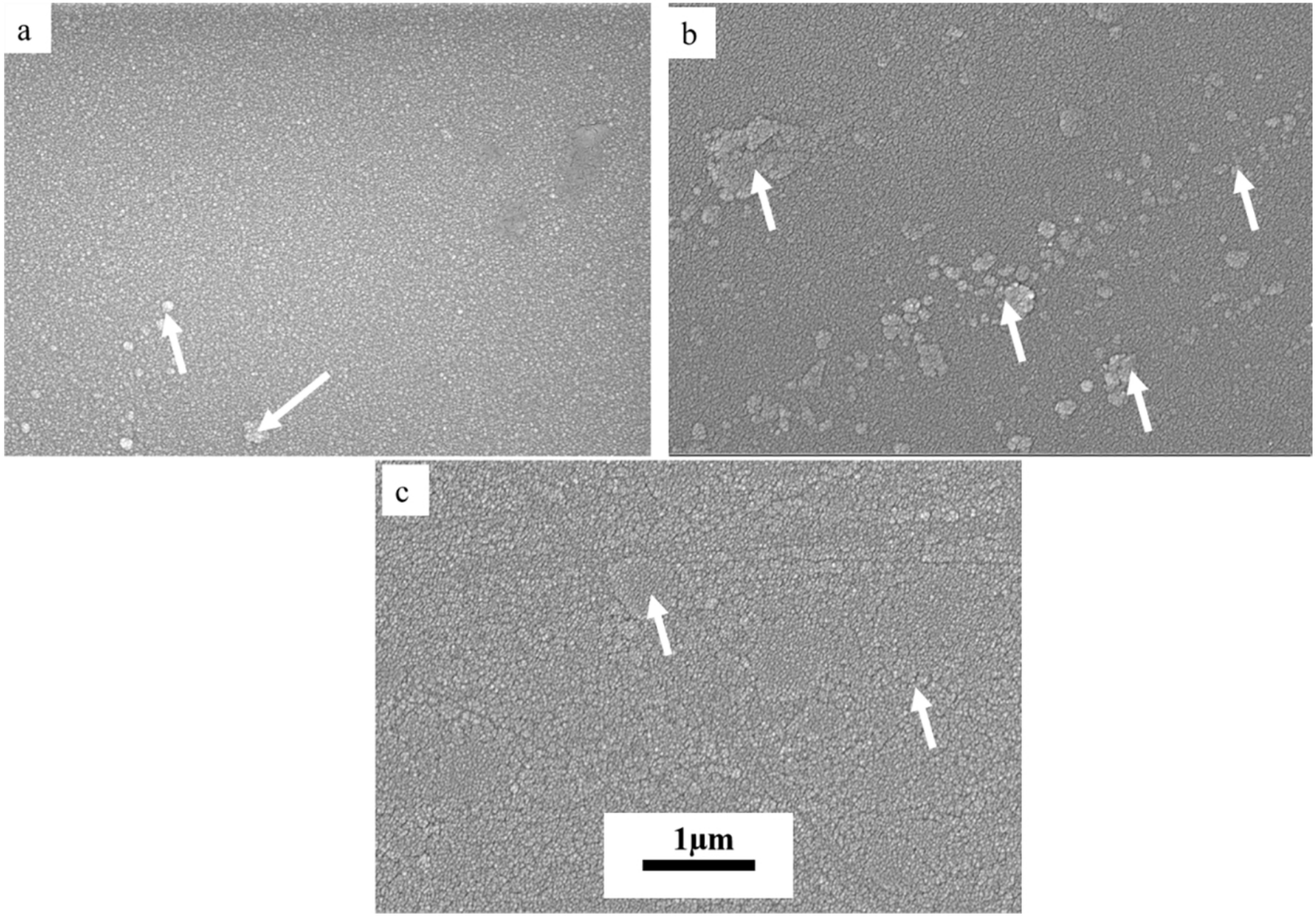

Figure 2

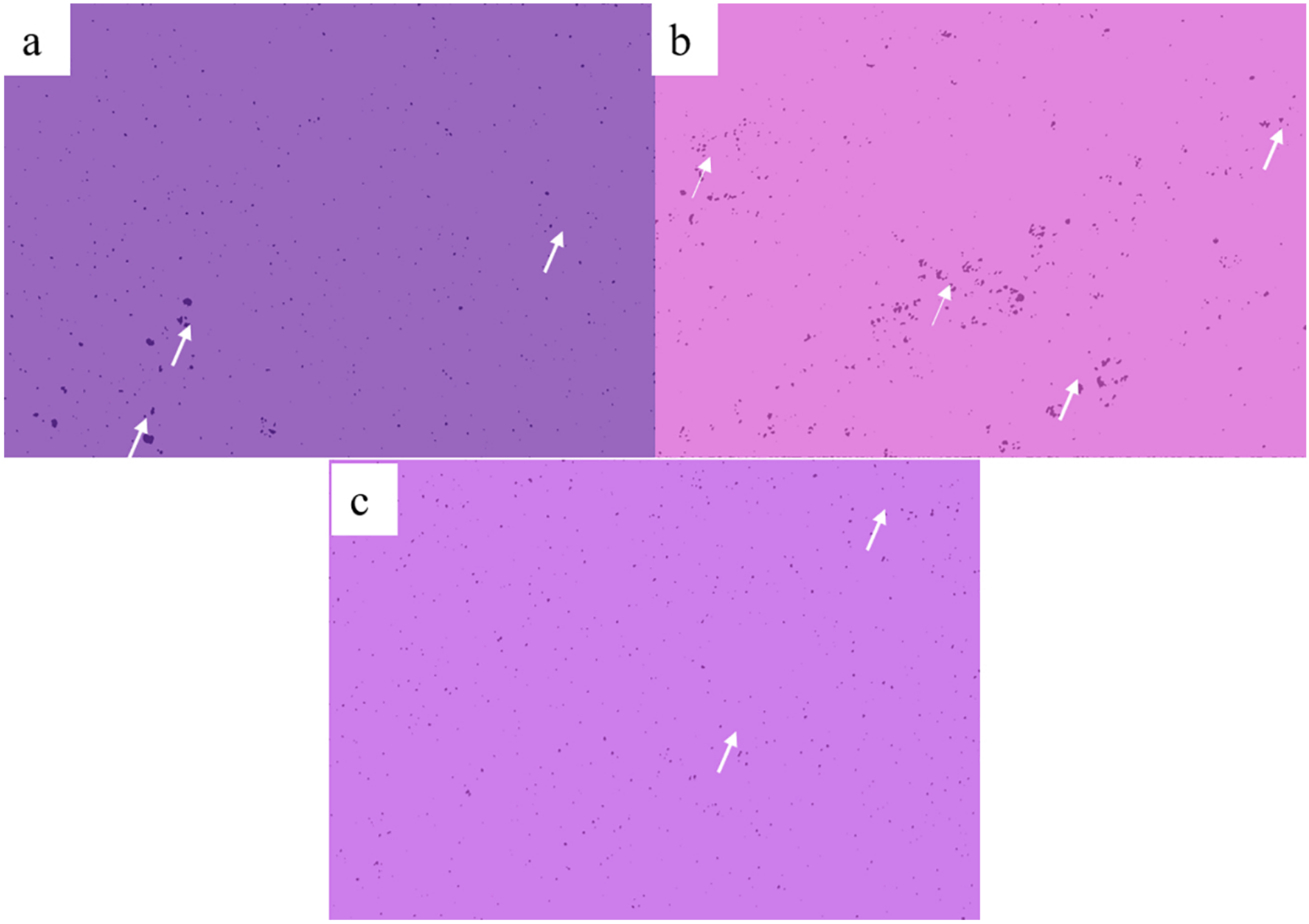

Figure 3

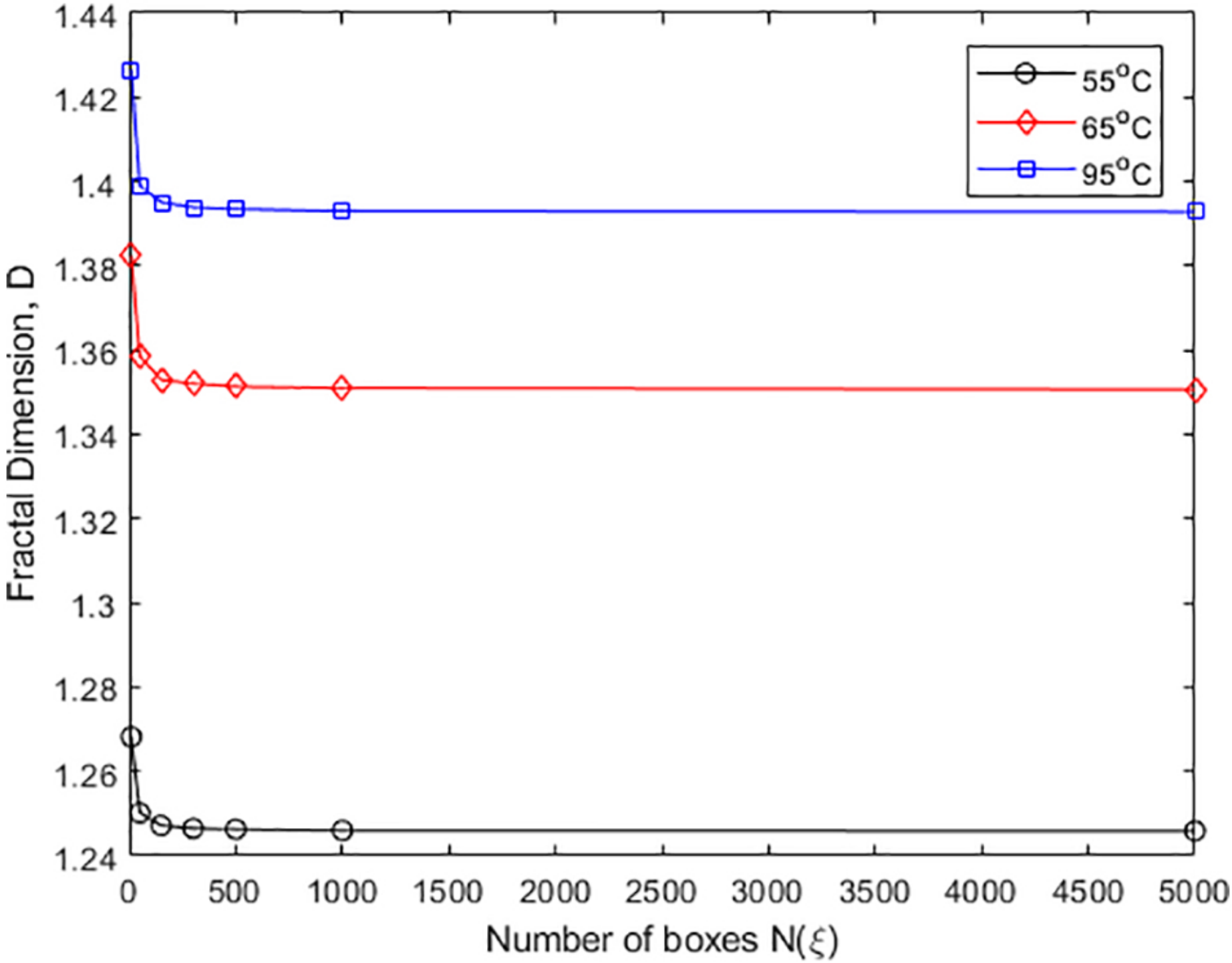
1.44
1.42
1.4
1.38
1.36
1.34
1.32
1.3
1.28
1.26
1.24
Fractal Dimension, D
0
500
1000
1500
2000
2500
3000
3500
4000
4500
5000
Number of boxes N(ξ)
55°C
65°C
95°C

Figure 4

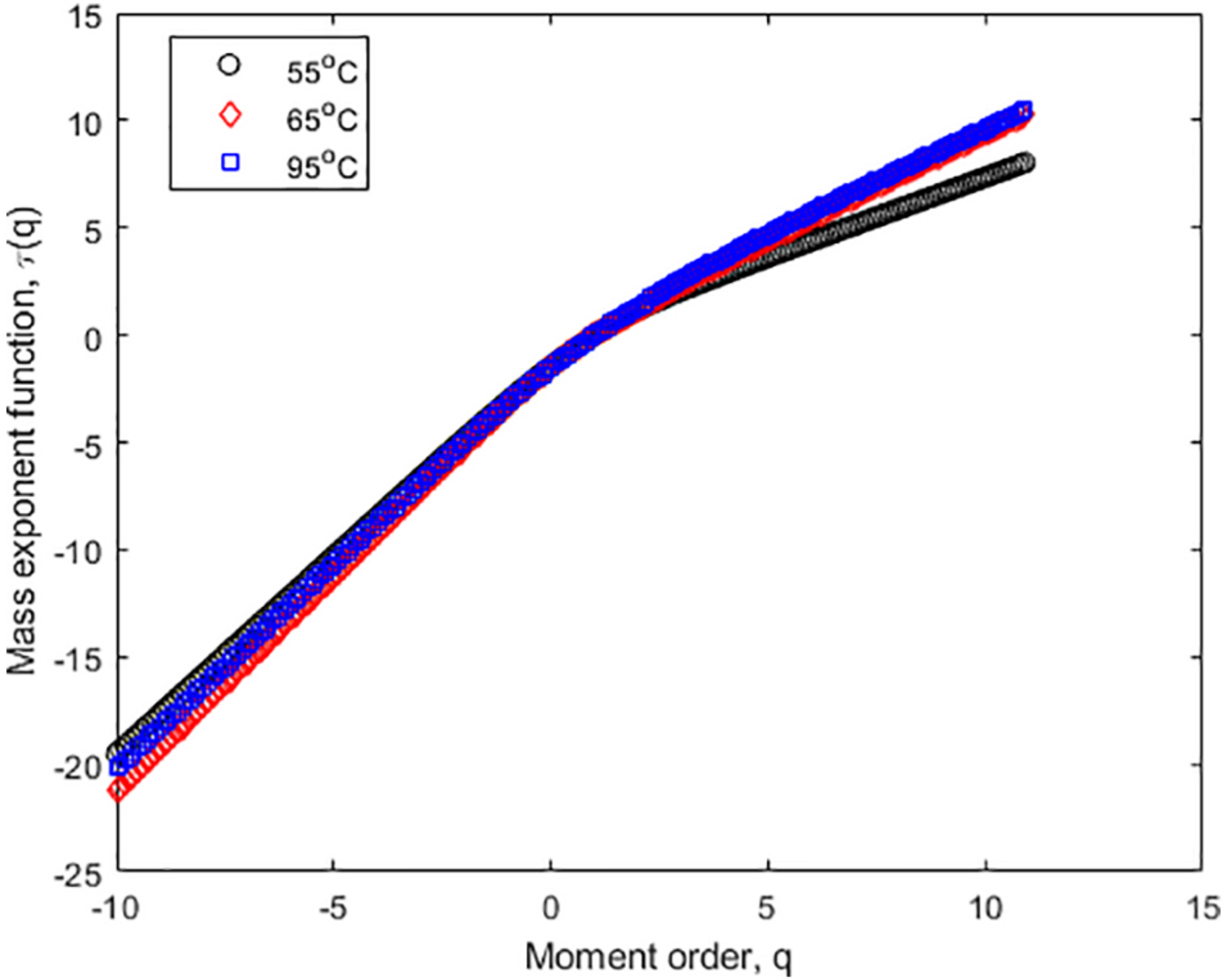
55°C
65°C
95°C
Mass exponent function, τ(q)
Moment order, q
15
10
5
0
-5
-10
-15
-20
-25
-10
-5
0
5
10
15

Figure 5

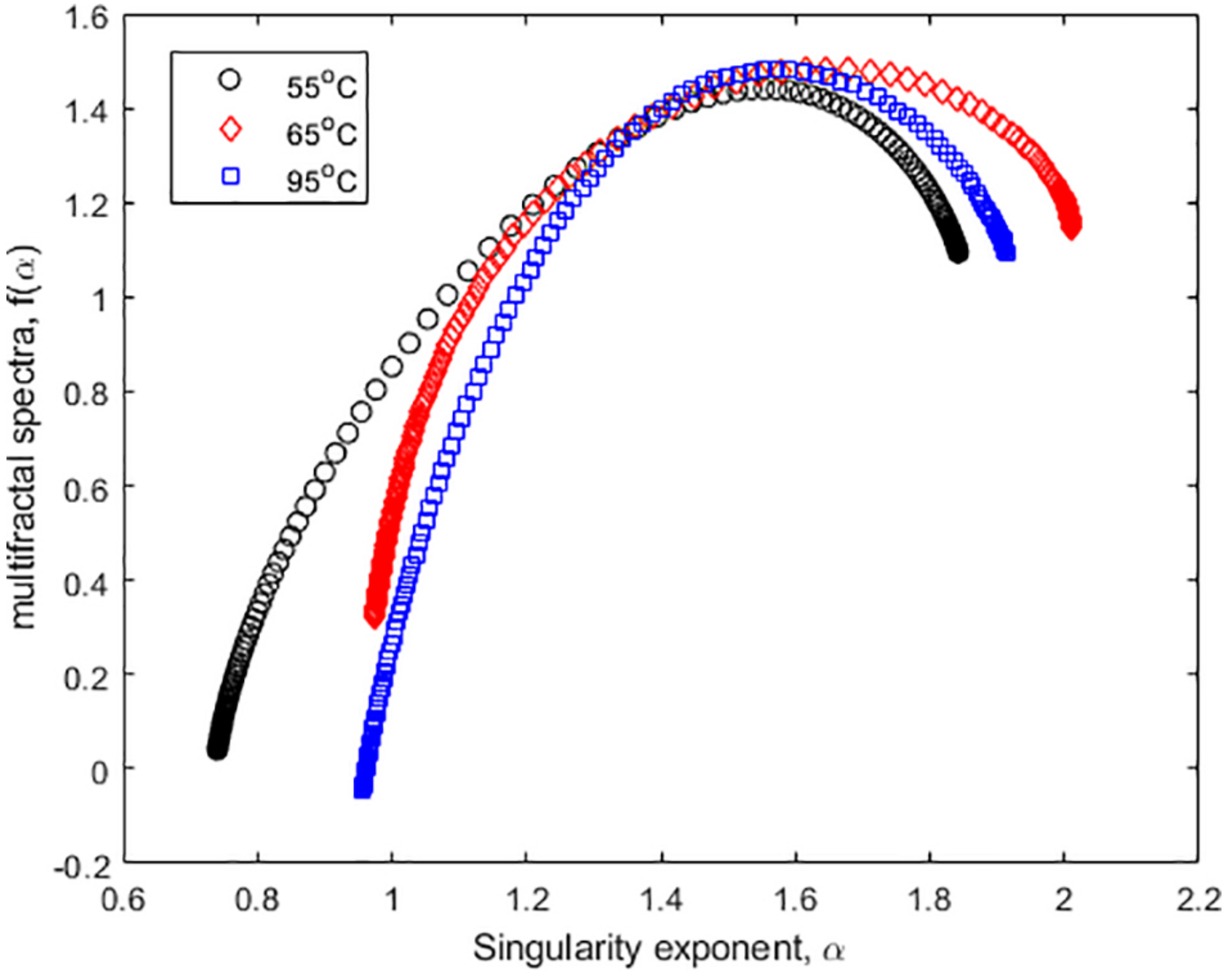
55°C
65°C
95°C
multifractal spectra, f(α)
Singularity exponent, α
1.6
1.4
1.2
1
0.8
0.6
0.4
0.2
0
-0.2
0.6
0.8
1
1.2
1.4
1.6
1.8
2
2.2

Figure 6

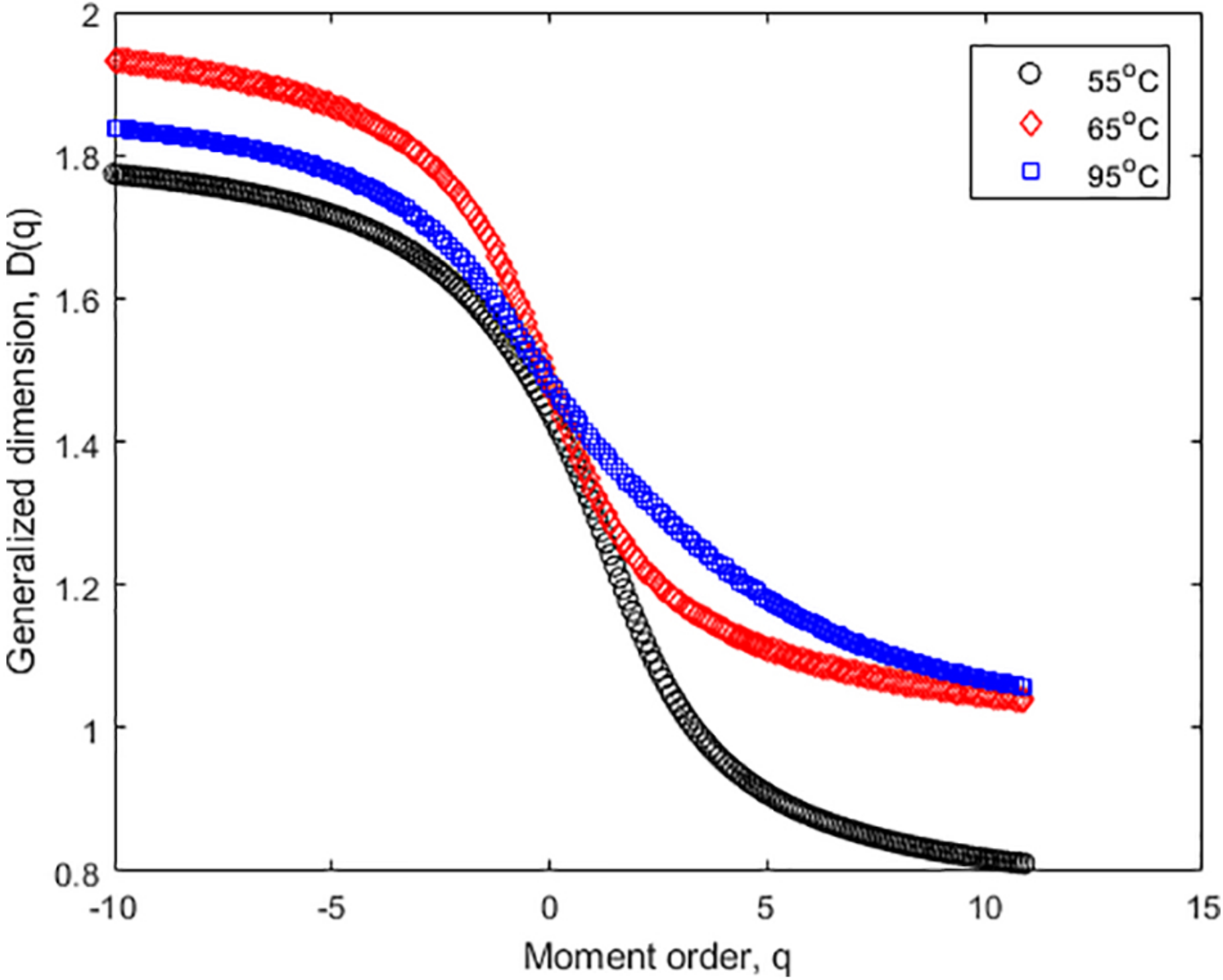
55°C
65°C
95°C
Generalized dimension, D(q)
Moment order, q
2
1.8
1.6
1.4
1.2
1
0.8
-10
-5
0
5
10
15

Figure 7

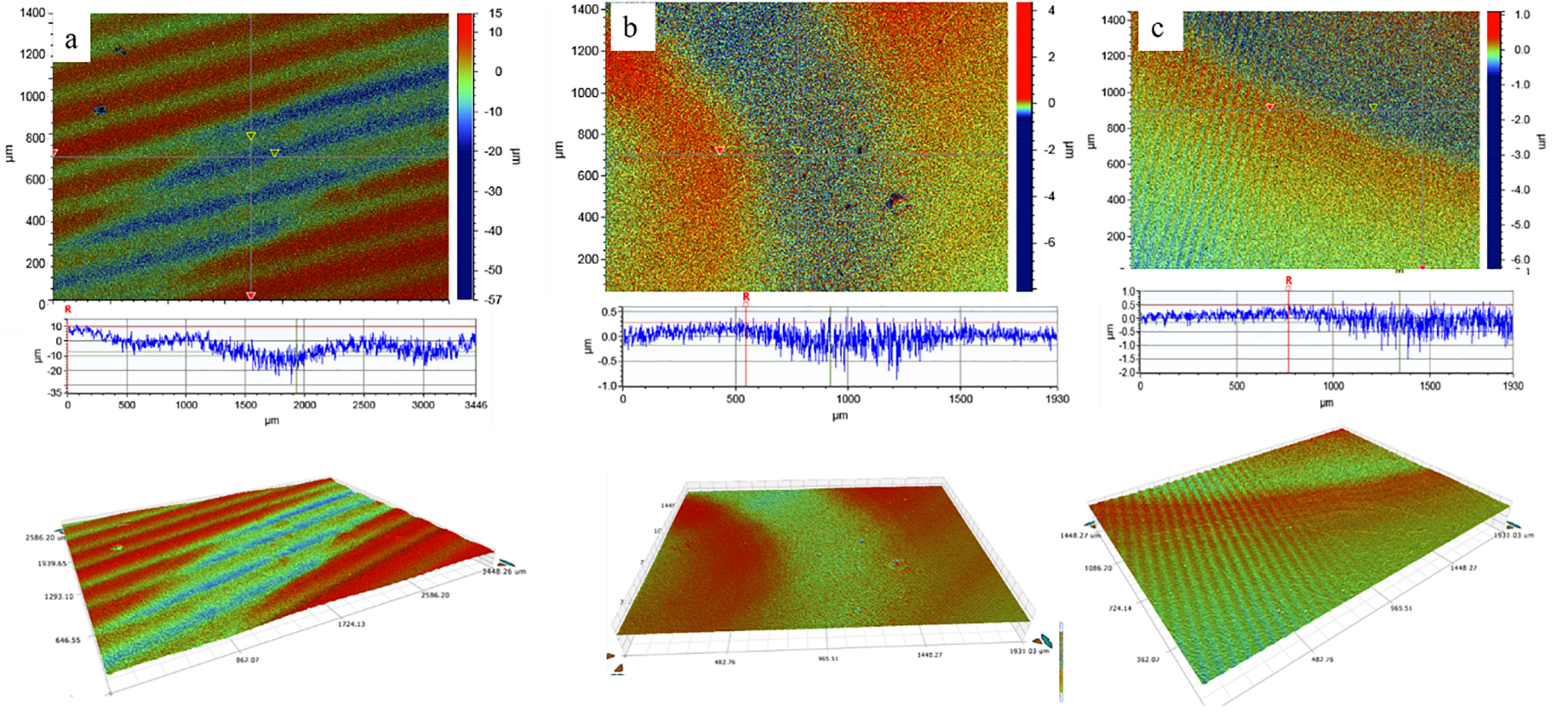

Figure 8

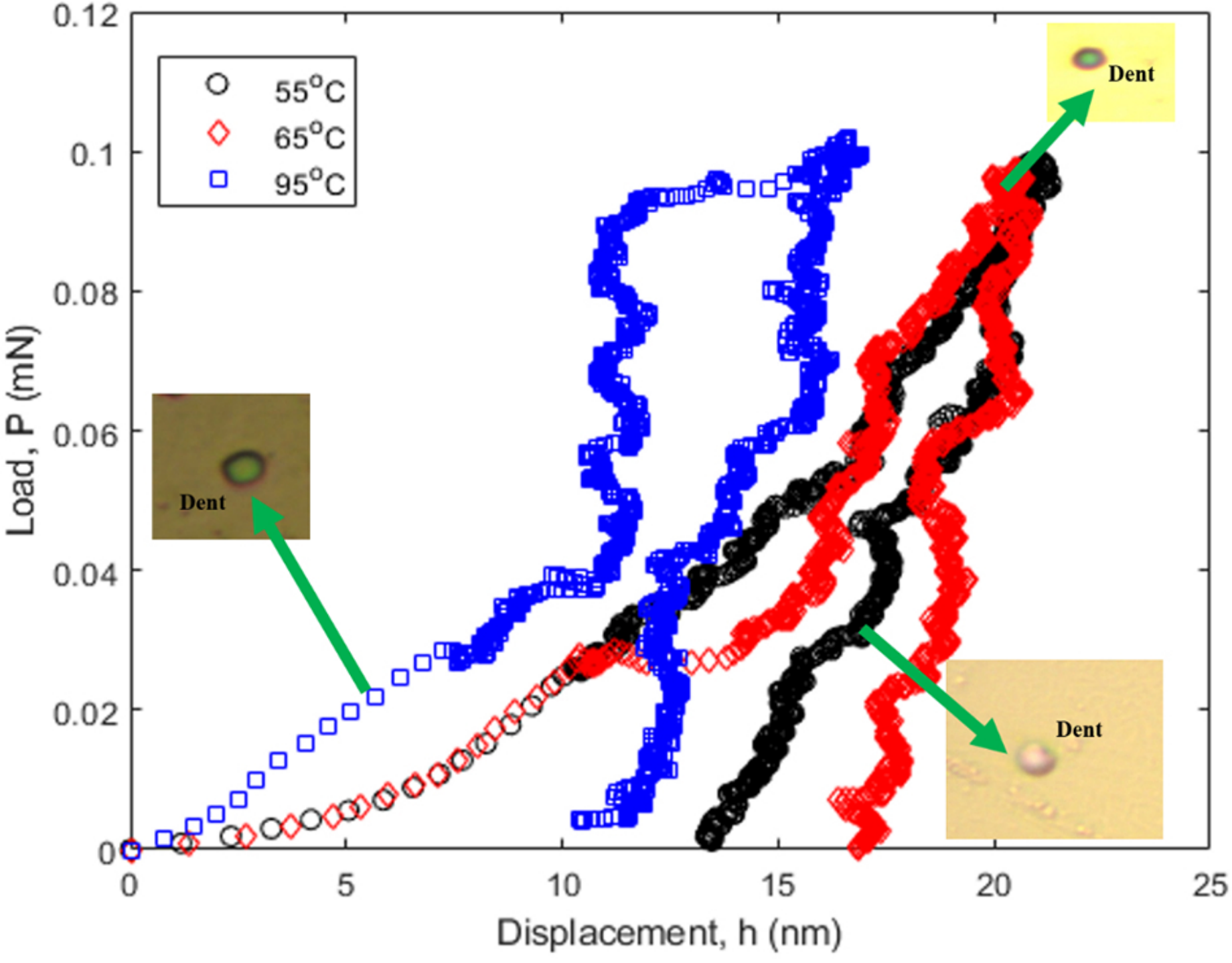
55°C
65°C
95°C
Dent
Dent
Dent
Load, P (mN)
Displacement, h (nm)
0.12
0.1
0.08
0.06
0.04
0.02
0
0
5
10
15
20
25

Figure 9